Nano-electrochemistry & Nano-photochemistry
https://www.sciltp.com/journals/nenp

Article

CuMg Alloy Catalyst for Electrochemical Dopamine Detection

Cheng Wang [1,2], Wenlong Xu [3], Yiming Zhang [4], Xun Zhang [4], Congxiao Wang [1,*] and Lei Jiao [4,*]

[1] Department of Interventional Medical Center, the Affiliated Hospital of Qingdao University, Qingdao 266000, China
[2] Suzhou Torckin Technology Co., Ltd., Suzhou 215400, China
[3] Harbin Boao Environmental Technology Co., Ltd., Qingdao 266061, China
[4] College of Chemistry and Chemical Engineering, Qingdao University, Qingdao 266071, China
* Correspondence: wcxguyu@163.com (C.W.); jiaolei@qdu.edu.cn (L.J.)

How To Cite: Wang, C.; Xu, W.; Zhang, Y.; et al. CuMg Alloy Catalyst for Electrochemical Dopamine Detection. *Nano-electrochemistry & Nano-photochemistry* **2026**, *2*(1), 3. https://doi.org/10.53941/nenp.2026.100003

Received: 11 December 2025
Revised: 29 January 2026
Accepted: 6 February 2026
Published: 13 February 2026

Abstract: Electrochemical sensors offer rapid, cost-effective, and portable detection but often suffer from narrow linear ranges and poor long-term stability due to catalyst degradation or surface fouling. Herein, an electrochemical sensor employing a Cu_1Mg_1 bimetallic alloy catalyst was developed for highly sensitive and rapid detection of dopamine (DA). The Cu_1Mg_1 alloy, synthesized via a facile method, exhibited enhanced electrocatalytic activity due to synergistic effects between Cu and Mg, optimizing electron transfer and surface reactivity. The sensor demonstrated a wide linear range (0.01–100 μM) and excellent selectivity against common interferents. Notably, it achieved rapid response and superior long-term stability. Mechanistic studies revealed that Mg's role in stabilizing Cu active sites and enhancing the conductivity was pivotal for broad-range detection. This work highlights the potential of Cu_1Mg_1 alloys as efficient catalysts for real-time, reliable neurotransmitter monitoring in biomedical applications, providing theoretical guidance for understanding the structure–property relationship.

Keywords: Cu_1Mg_1 alloy catalyst; dopamine; electrochemical sensor; depression

1. Introduction

Depression stands as one of the most prevalent and debilitating mental health disorders worldwide, imposing a substantial burden on individuals, families, and society at large [1,2]. According to the World Health Organization (WHO), depression affects over 264 million people globally, leading to a significant decline in quality of life, increased morbidity, and in severe cases, suicide [3,4]. Unraveling the underlying pathophysiological mechanisms of depression and developing effective diagnostic and therapeutic strategies are of paramount importance in the field of mental health research. To date, the diagnosis of depression is largely dependent on clinical interviews and questionnaires [5,6]. The lack of a reliable biomarker for depression limits the confirmation of diagnosis, as well as the assessment of treatment and prognosis [6]. A potential biomarker may also serve as a probe for elucidating the pathogenesis of disease or a target for developing new therapeutic interventions [6–8]. Dopamine (DA) plays a pivotal role in the pathophysiology of depression, primarily through its involvement in the brain's reward circuitry [7,9]. A growing body of evidence has firmly established a strong link between depression and dysregulation of the dopaminergic system [10,11]. Dysregulation of dopaminergic signaling—characterized by reduced synthesis, impaired receptor sensitivity, or disrupted neural connectivity—has been linked to core depressive symptoms, including anhedonia (loss of pleasure), diminished motivation, and cognitive deficits [12–15]. The accurate measurement of DA is of great significance for neurogenic diseases. Therefore, accurate and sensitive detection of

dopamine levels in biological samples holds great promise for enhancing our understanding of depression pathogenesis, enabling early diagnosis, and monitoring treatment efficacy [16,17].

Numerous analytical techniques have been developed for DA detection, such as high-performance liquid chromatography assay [18–20], spectrophotometric assay [21], and enzyme-linked immunosorbent assay [22,23]. After many years of development of these approaches, the sensitivity and the accuracy both reach very high level. However, the complicated operation, expensive instrumentations and expert technical limited the efficiency and cost of sensitive detection. On the other hand, the electrochemical methods have attracted significant attention for DA detection due to their inherent advantages, such as simplicity, cost-effectiveness, rapid response, and high sensitivity. Particularly, the oxidation process of DA exhibits high specificity due to its unique redox potential and structural features, allowing precise quantification even in complex biological samples. So, the quantitative analysis based on the electrocatalytic oxidation signal of DA has emerged as a promising approach. When DA undergoes electrocatalytic oxidation at the electrode surface, an electrical signal is generated that is directly proportional to its concentration. However, conventional electrochemical sensors face challenges in achieving high selectivity and anti-interference ability, especially in complex biological matrices where various co-existing substances, such as ascorbic acid (AA) and uric acid (UA), have similar oxidation potentials to DA, leading to signal overlap and inaccurate quantification.

In recent years, the improvement in electrochemical sensing performance has been largely attributed to the precise control over the composition and microstructure of nanomaterials. Polymer nanocomposites combine the flexibility of polymers with the high conductivity, large specific surface area, and other advantageous properties of nanomaterials, making them widely applicable in biosensing [24]. Fluorescent molecularly imprinted polymers possess high selectivity and tunable fluorescence characteristics, enabling the specific recognition and fluorescent response of target molecules in complex matrices [25]. Graphene quantum dots and their functionalized derivatives leverage quantum confinement and edge effects to exhibit significantly enhanced optoelectronic properties [26]. These advancements provide an important paradigm for the rational design of functional nanomaterials. However, in the context of dopamine electrooxidation and its sensing applications, how to precisely regulate the electronic and geometric structures of catalysts to deeply reveal their structure–activity relationships remains a critical challenge [27–29].

Against this background, bimetallic alloy catalysts have attracted widespread attention due to their demonstrated synergistic effects. Such synergistic effects can significantly enhance the catalytic activity, selectivity, and stability of the system. By constructing alloy systems such as Ag–Cu and Cu–Zn, it is possible to optimize oxygen activation, substrate adsorption, and resistance to deactivation, thereby enabling efficient applications in environmental and industrial catalytic processes [30,31]. Among various bimetallic systems, copper-magnesium (Cu–Mg) catalysts exhibit unique research value. As a transition metal, copper possesses excellent intrinsic electrocatalytic activity and conductivity, providing abundant active sites for dopamine oxidation reactions [32]. Magnesium, as an alkaline earth metal, exhibits limited catalytic activity on its own. However, when combined with copper to form a bimetallic structure, it can generate significant synergistic effects at the atomic scale [33–34]. This atomic-level interaction can effectively modulate the electronic structure of copper and optimize the electron density distribution around its active centers, making it a promising system that can be further regulated through nanostructure engineering. This holds potential for achieving higher reactivity and improved selectivity in the electrocatalytic oxidation of DA.

Herein, Cu_xMg_y alloy catalyst was prepared by the high-temperature annealing method to realize the detection of DA. Building on the superior performance of the Cu-Mg bimetallic catalyst, we successfully constructed an electrochemical sensor for rapid and highly sensitive DA detection. The nanostructured Cu_xMg_y alloy not only increased the surface area of the electrode, providing more active sites for DA adsorption and oxidation, but also facilitated efficient electron transfer, thereby enhancing the electrocatalytic efficiency. A series of electrochemical experiments was carried out to characterize and evaluate the performance of the constructed electrochemical sensor. The results demonstrated that the sensor exhibited an extremely high sensitivity for DA detection, with a detection limit reaching the nanomolar level, which is well below the physiological concentrations of DA in biological samples. Moreover, the sensor showed excellent selectivity, allowing for accurate quantification of DA in the presence of various interfering substances commonly found in biological fluids. The sensor also displayed a rapid response time and good long-term stability, making it suitable for real-time and continuous monitoring of DA levels.

2. Experimental Section

2.1. Reagents and Materials

The copper powder, magnesium powder, Nafion N-520, and Super P® Li carbon black were obtained from Alfa Aesar China Co., Ltd. (Shanghai, China). Dopamine (DA), zinc chloride ($ZnCl_2$), potassium chloride (KCl) and sodium chloride (NaCl) were obtained from Shanghai Maclin Biochemical Technology Co., Ltd. (Shanghai, China). Glucose, L(+)-Glutamic acid and L-Lysine were obtained from Aladdin Reagent (Shanghai) Co., Ltd. (Shanghai, China) All solutions were prepared using ultrapure water with an electric resistance >18.25 MΩ, which was obtained through a Millipore Milli-Q water purifiation system (Billerica, MA, USA).

2.2. Apparatus

The morphology and chemical components were characterized with scanning electron microscopy (SEM, Hitachi S-4800, Chiyoda City, Japan) and corresponding energy-dispersive spectroscopy (EDS). The crystal structure information of samples was collected by X-ray diffraction (Rigaku Smart Lab, Japan) with Cu Kα (λ = 1.541 Å) at the scan range of 2θ from 10° to 80°. The chemical compositions and valence states on the electrode surface were obtained by Xray photoelectron spectrometer (XPS) on an AXIS Supra spectrometer (Kratos Analytical Inc.) equipped with AXIS-HS monochromatic Al Kα cathode sources. All the XPS spectra were based on C1s (284.8 eV). Linear sweep voltammetry (LSV), Cyclic voltammetry (CV) measurements, electrochemical impedance spectroscopy (EIS), and differential pulse voltammetry (DPV) measurements were carried out using a CHI 660D electrochemical workstation (Shanghai CH Instruments, Shanghai, China). All experiments were performed using a conventional three-electrode system consisting of a Ag/AgCl reference electrode, a platinum wire auxiliary electrode, and a modified glassy carbon working electrode.

2.3. Preparation of Cu_xMg_y Alloy

The Cu_xMg_y alloy catalyst is mainly prepared through two steps. Firstly, the Cu source and Mg source are dispersed and mixed to form a precursor. The copper source is commercial copper powder (325 mesh), and the magnesium source is magnesium powder (200 mesh). Then, the precursor is subjected to high-temperature annealing to obtain the target product. The specific synthesis steps are as follows: Firstly, a certain amount of commercial copper powder and magnesium powder, as well as Super P® Li carbon black, are added to 5 mL of acetone solution. Then, the suspension is ultrasonically heated to 50 °C, and ultrasonic stirring is carried out to ensure uniformity. The acetone solution is completely evaporated, and the solid mixture is fully ground. The solid mixture is then heated in a H_2/Ar (*v*:*v* = 5%:95%) atmosphere at 700 °C for 4 h at a heating rate of 10 °C/min. After the calcination is completed, the Cu_xMg_y alloy catalyst can be obtained. Cu_xMg_y catalysts can be prepared by regulating different Cu/Mg ratios (1:0, 1:1, and 0:1), where x and y represent the molar quantities of Cu and Mg.

3. Results and Discussion

3.1. Characterization of Cu_xMg_y Alloy

The Cu_xMg_y alloy catalysts are mainly prepared by the calcination of the copper powder (325 mesh) and the magnesium powder (200 mesh) (Figure 1a). The specific procedure can be found in the experimental synthesis section. As a comparison, Cu_1Mg_0 and Cu_0Mg_1 were also synthesized following a procedure similar to that of Cu_1Mg_1. As shown in Figure 1b–d, it was found that the overall structure of all the Cu_xMg_y catalysts was spherical in shape. The Cu_1Mg_0 catalyzes the formation of nanoparticles stacked at around 40–50 nm, while for the Cu_1Mg_1 catalyst, nanoparticles of 20–40 nm are stacked. To accurately investigate the specific changes in the particle size of the catalysts, the particle size distribution analysis of the spherical structures of SEM for each catalyst was conducted. As shown in Figure S1, the particle size of the Cu_1Mg_0 catalyst mainly falls within the range of 42.3 ± 0.8 nm, while the particle sizes of the Cu_1Mg_1 catalyst were concentrated at 31.8 ± 0.8 nm. With the increase in Mg content, the particle size of the catalyst particles shows a significant reduction trend. This change leads to an increase in the active surface area of the catalyst, thereby exposing more active sites. From the dispersion state of the nanoparticles, for the pure Cu catalyst, its spherical nanoparticles are relatively aggregated. After adding Mg to form CuMg alloy, at this time, the spherical nanoparticles become more dispersed, which further indicates that the addition of Mg makes Cu more dispersed, providing a larger specific surface area and more active sites for the subsequent electrocatalytic oxidation of DA. Figure 1e shows the X-ray diffraction spectrum result of the Cu_1Mg_1 catalyst, its main peak was highly consistent with Cu_2Mg (PDF#01-1226), and it only contained a trace amount of $CuMg_2$ (PDF#13-0504) inclusions.

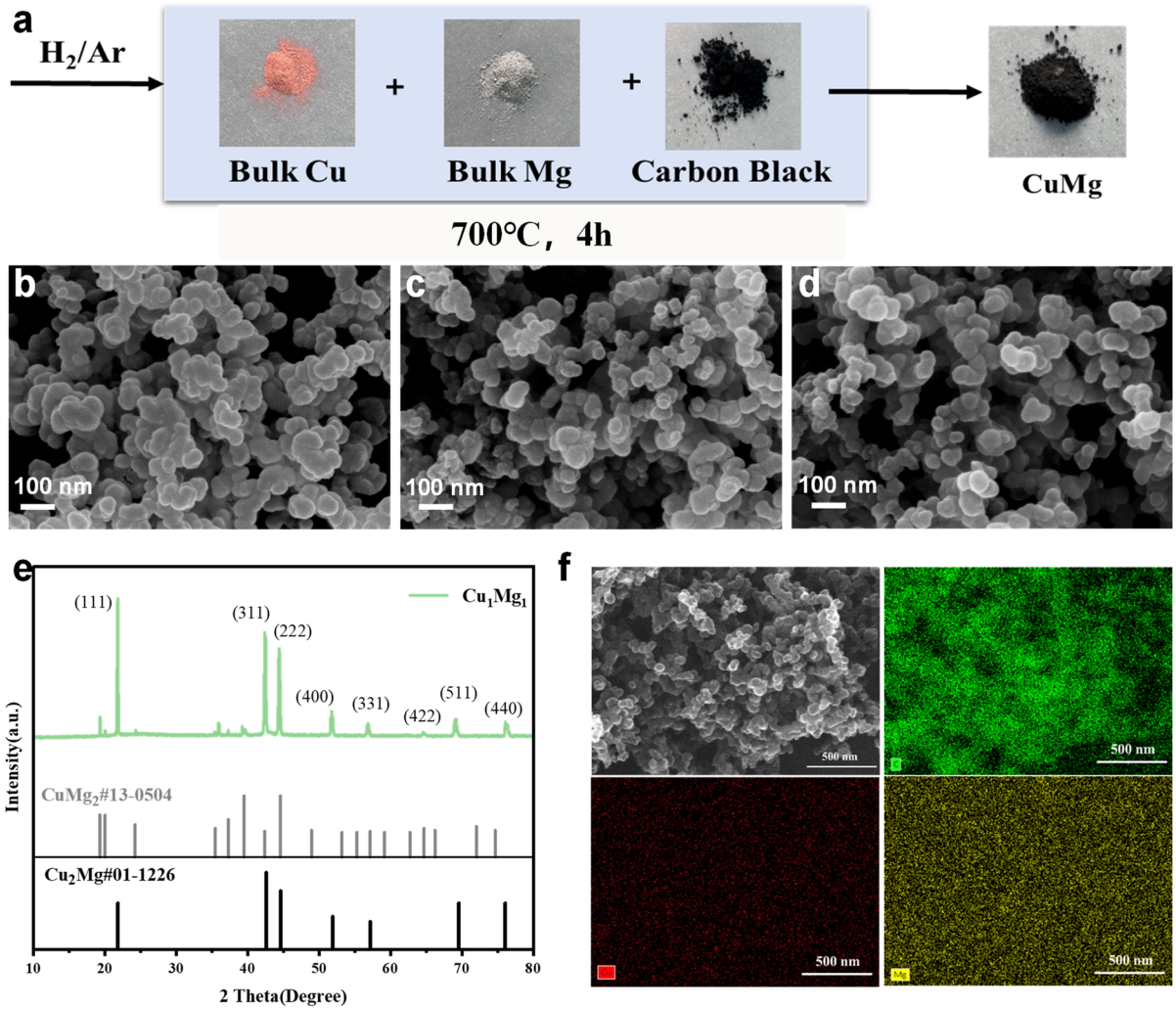

Figure 1. (**a**) Schematic synthesis of Cu_xMg_y alloy catalysts. The SEM images of Cu_1Mg_0 (**b**), Cu_1Mg_1 (**c**), and Cu_0Mg_1 (**d**). (**e**) The XRD image of Cu_1Mg_1 catalyst. (**f**) The EDS mapping images of the Cu_1Mg_1 catalyst.

Based on the SEM-EDS imaging images in Figure 1f, it can be found that the elements of C, Cu, and Mg are uniformly distributed in the Cu_1Mg_1 material, indicating that no other impurities have been introduced during the synthesis of the catalyst.

The valence states and inter-electronic interactions of surface elements in Cu_xMg_y catalysts were investigated by X-ray photoelectron spectroscopy (XPS) technology. As shown in Figure 2a, a full-spectrum scan was conducted on the Cu_xMg_y catalyst system. The spectral analysis revealed characteristic peaks of Cu, Mg, and C, and no characteristic signals of other elements were observed within the detection limit, confirming that no impurity atoms were introduced in the prepared catalyst. By analyzing the spectra of the Cu 2*p* and Mg 1*s* orbitals, characteristic peaks were observed at binding energies of 932.6 eV, 952.4 eV, and 1303 eV. As shown in Figure 2b,c, further peak fitting of Cu 2*p* indicates that Cu 2*p* corresponds to the metallic copper (Cu^0) state at 932.6 eV and 952.4 eV, while the peak fitting of Mg 1*s* shows that Mg 1*s* at 1303 eV corresponds to the metallic magnesium (Mg^0) state. The valence state of the elements determined by XPS is consistent with the results of XRD analysis. By comparing the binding energies of the Cu 2*p* orbitals of the Cu_1Mg_1 and Cu_1Mg_0 samples, it was found that their binding energies shifted towards lower binding energies. And for the Mg 1s binding energy, compared with Cu_0Mg_1, shows a shift towards a higher binding energy. This indicates that Mg transfers electrons to Cu, and Mg enhances the electron cloud density distribution of Cu through electron transfer, forming a strongly coupled bimetallic cooperative system. In the CuMg bimetallic system, the introduction of metal Mg effectively enhances the electron interaction between the CuMg bimetallic components.

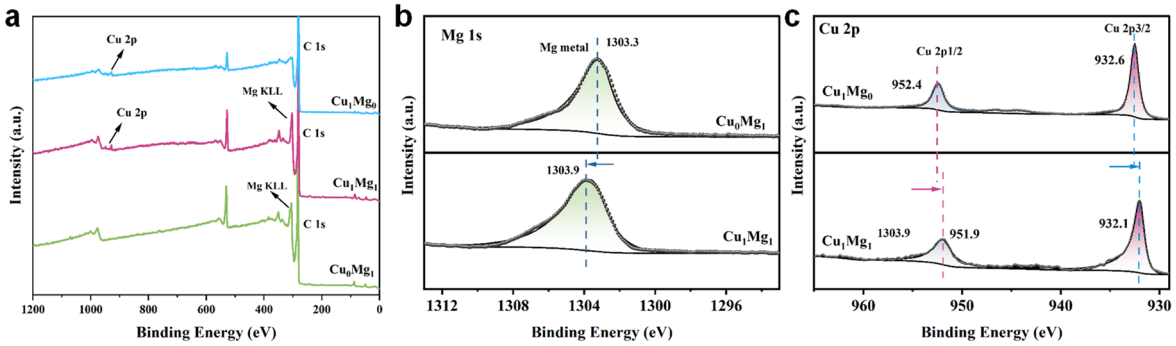

Figure 2. (**a**) XPS survey spectra of Cu_1Mg_0, Cu_0Mg_1 and Cu_1Mg_1, (**b**) Mg 1*s* spectra of Cu_0Mg_1 and Cu_1Mg_1, (**c**) Cu 2p spectra of Cu_1Mg_0 and Cu_1Mg_1.

3.2. Electrochemical Responses of DA Oxidation

The DA molecule is chosen as the model to explore the biomolecular oxidation performance. Before the evaluation of the electrochemical responses of Cu_xMg_y for DA oxidation, a comparative analysis of the charge transfer properties is initially conducted. Using $[Fe(CN)_6]^{3-/4-}$ as a redox probe, the redox current response of Cu_1Mg_1 is the highest among the three prepared catalysts, indicating the most outstanding electrocatalytic performance (Figure S2). As displayed by the cyclic voltammetry (CV) responses in Figure 3a, well-resolved redox peaks appeared upon adding DA (100 μM) into the electrolyte. In detail, the peak intensity for the Cu_1Mg_0 catalyst is the lowest, and the peak intensity for the Cu_0Mg_1 is obviously higher than that of the Cu_1Mg_0 catalyst. While the Cu_1Mg_1 catalyst showed the strongest peak intensity, which is in agreement with the result shown in Figure S2. The electrochemical impedance spectroscopy (EIS) is used to characterize the resistance of charge transfer. As shown in Figure 3b, the glassy carbon electrode (GCE) has the largest radius, indicating that the resistance of charge transfer is the greatest. The important thing is that the impedance radius gradually decreases with the modification of the catalyst on the surface of the GCE. Among them, the Cu_1Mg_1 catalyst exhibited the smallest radius, demonstrating its outstanding charge transport capability. The wide potential window, according to the linear sweep voltammetry (LSV) curve, ensures that there are no interfering reactions during the DA oxidation in Figure 3c.

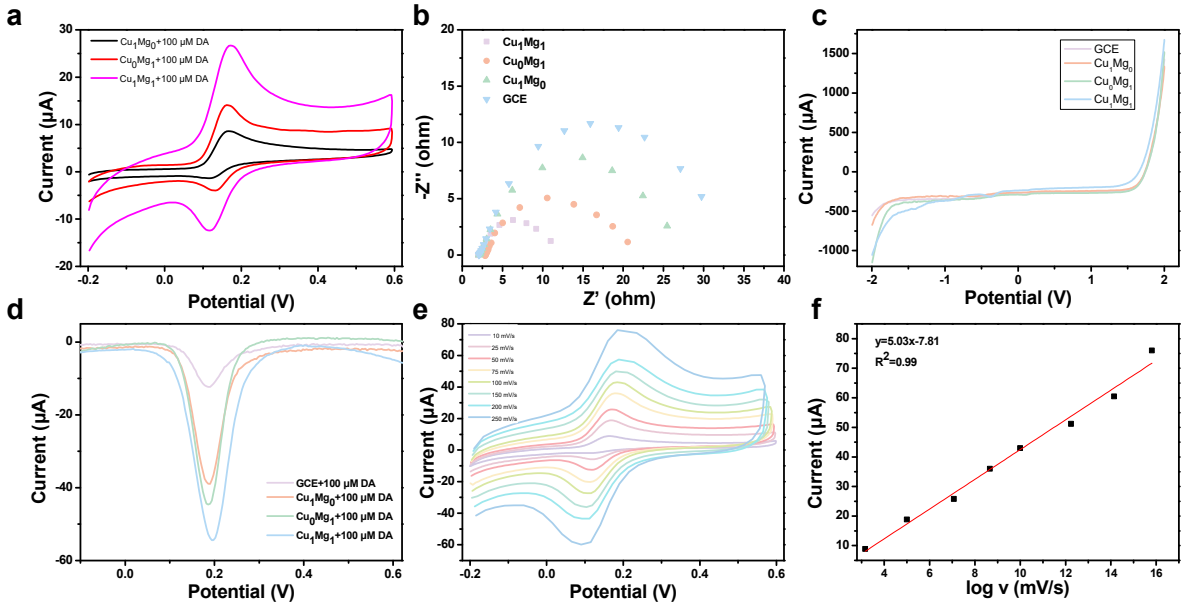

Figure 3. (**a**) CV curves of Cu_xMg_y catalysts modified electrodes with 100 μM DA, (**b**) EIS in $[Fe(CN)6]^{3-/4-}$ of pure GCE and Cu_xMg_y catalysts modified electrodes, (**c**) LSC curves of pure GCE and Cu_xMg_y catalysts modified electrodes, (**d**) DPV responses with 100 μM DA in PBS (0.1 M, pH = 7.4), (**e**) CV curves of Cu_1Mg_1 with different scan rates (10–250 mV/s) in 100 μM of DA. (**f**) Standard curve of the CV peak redox potential and the logarithm of the scan rate for Cu_1Mg_1.

Differential pulse voltammetry (DPV) was carried out to explore the electrochemical responses of Cu_xMg_y catalysts for DA oxidation. In Figure 3d, there is an obvious electrochemical signal at 0.20 V in 0.1 M PBS (pH = 7.4) containing 100 μM DA, which belongs to the electrochemical oxidation signal of DA. It can be seen that electrodes modified with Cu_xMg_y catalysts exhibit better sensitivity for the electrochemical oxidation of DA than the GCE. The Cu_1Mg_1 catalyst has the highest oxidation current density under the same DA concentration (100 μM), indicating the highest sensitivity for the electrochemical oxidation of DA. CV tests were performed on Cu_1Mg_1 catalyst at different scanning rates to further study the electron transfer kinetics of DA oxidation (Figure 3e). The peak currents of the oxidation peak and reduction peak of Cu_1Mg_1 catalyst increase gradually with increasing scanning rate. As shown in Figure 3f by fitting the linear relationship between their oxidation peak current and the square root of the scanning rate, the DA oxidation process is controlled by the diffusion process.

3.3. Electrochemical DA Detection

Based on the above mentioned investigation, a sensitive DA electrochemical sensor was established. Figure 4a depicts typical DPV responses of the biosensor to DA of varying concentrations. We observed dynamically increased DPV peaks in response to DA of increasing concentrations within the range from 1×10^{-2} to 100 μM. The relationship between concentration and peak current value is shown in Figure 4b, and a linear model I = 0.54c + 1.42, where I (10^{-6} A) is the peak current intensity and C (μM) is the concentration of DA. The R^2 is 0.998 for the standard equation, indicating that the sensing strategy could be used for quantitative analysis of DA.

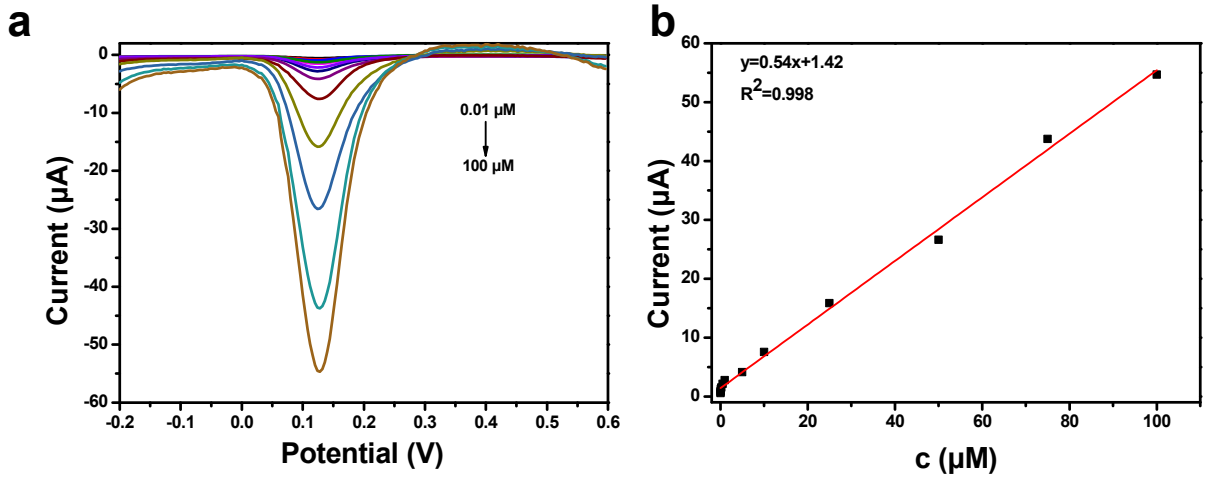

Figure 4. (**a**) DPV responses for various concentrations of DA of Cu_1Mg_1 modified electrodes. (**b**) Calibration curve of DA detection.

3.4. The Selectivity, Reproducibility, and Stability of the Biosensor

As for practical sensing applications, the anti-interference ability, selectivity, stability, and repeatability are also investigated. Amino acids, glucose, and metal ions are selected as interfering substances. The electrochemical responses in Figures 5a,b reveal that the proposed electrochemical sensor has excellent selectivity. In addition, after one month, the electrochemical sensor can maintain 94.64% of its initial responses, which indicates that the electrochemical sensor exhibits satisfactory stability (Figure 5c). As shown in Figure 5d, after recurrent usage for 5 times, 93.50% of the electrochemical responses for the electrochemical sensor are still retained, indicating its excellent repeatability.

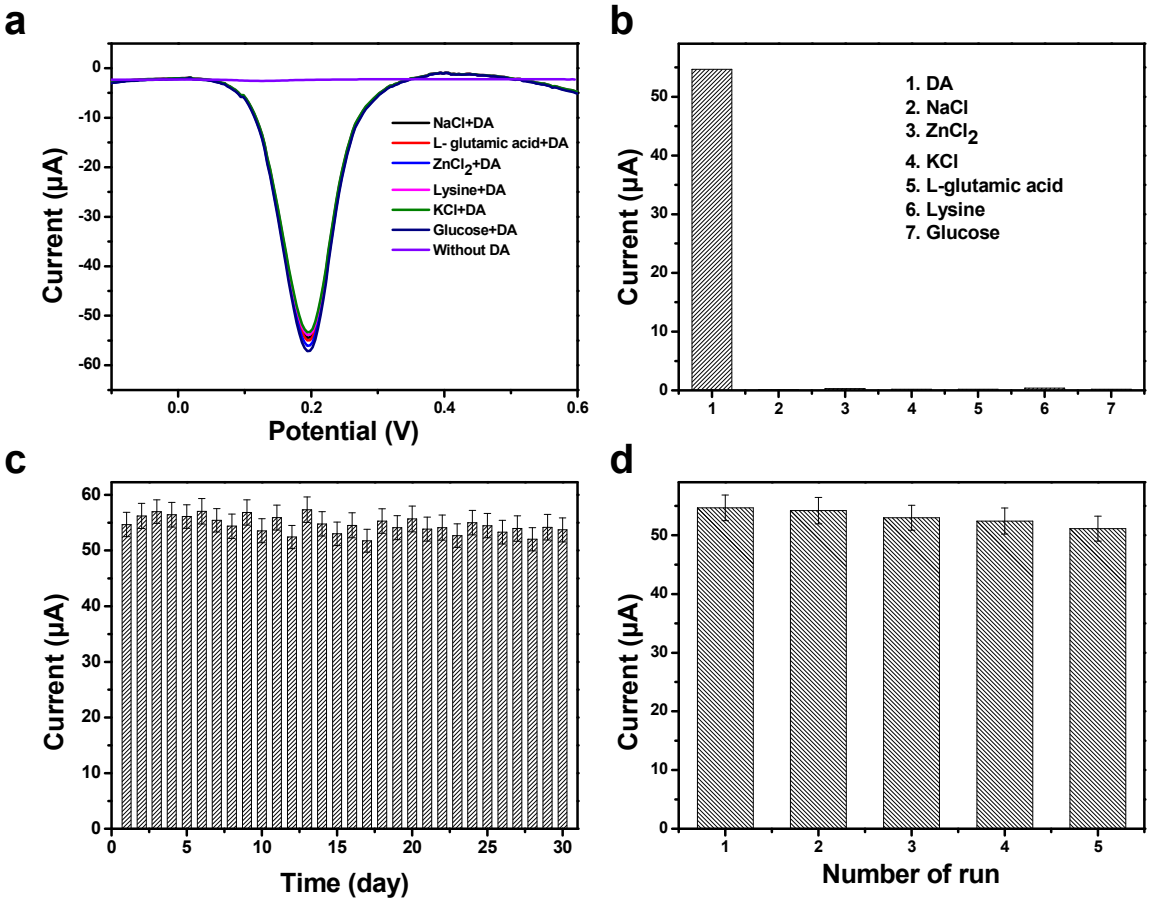

Figure 5. (**a**) Anti-interference ability of Cu_1Mg_1 towards DA detection. (**b**) Selectivity of Cu_1Mg_1 towards DA detection. (**c**) Stability of Cu_1Mg_1 towards DA detection. (**d**) Reusability measurements of Cu_1Mg_1 towards 100 μM DA upon recurrent usage for 5 times.

4. Conclusions

In summary, this study addresses the critical need for highly sensitive and selective detection of DA in the context of depression research. By comparing different metal catalysts, we identified the Cu-Mg bimetallic catalyst as an optimal choice for enhancing the electrocatalytic performance of DA oxidation. The construction of an electrochemical sensor based on this bimetallic catalyst provides a reliable and efficient tool for rapid and highly sensitive dopamine detection, which has the potential to significantly advance our understanding of depression pathophysiology and improve clinical diagnosis and treatment strategies.

Supplementary Materials

The additional data and information can be downloaded at: https://media.sciltp.com/articles/others/2602121714198456/NENP-25120090-Supplementary_Materials.pdf. Figure S1. The particle size distribution graphs of Cu_1Mg_0 (a), Cu_1Mg_1 (b), and Cu_0Mg_1 (c). Figure S2. CV curves of Cu_xMg_y catalysts in $[Fe(CN)_6]^{3-/4-}$ solution.

Author Contributions

C.W. (Cheng Wang): data curation, writing—original draft preparation; W.X.: investigation; Y.Z. and X.Z.: writing—reviewing and editing; C.W. (Congxiao Wang) and L.J.: supervision. All authors have read and agreed to the published version of the manuscript.

Funding

This work was supported by the Natural Science Foundation of Shandong Province (ZR2023QB006).

Data Availability Statement

Data will be made available on request.

Conflicts of Interest

The authors declare no conflict of interest.

Use of AI and AI-Assisted Technologies

No AI tools were utilized for this paper.

References

1. Zhang, J.; Liu, D.; Xiang, J.; et al. Combining Glial Fibrillary Acidic Protein and Neurofilament Light Chain for the Diagnosis of Major Depressive Disorder. *Anal. Chem.* **2024**, *96*, 1693–1699.
2. Xiu, J.; Li, J.; Liu, Z.; et al. Elevated BICD2 DNA methylation in blood of major depressive disorder patients and reduction of depressive-like behaviors in hippocampal $Bicd_2$-knockdown mice. *Proc. Natl. Acad. Sci. USA* **2022**, *119*, e2201967119.
3. Shi, Y.; Song, R.; Wang, L.; et al. Identifying Plasma Biomarkers with high specificity for major depressive disorder: A multi-level proteomics study. *J. Affect. Disord.* **2020**, *277*, 620–630.
4. Zhang, G.; Li, L.; Kong, Y.; et al. Vitamin D-binding protein in plasma microglia-derived extracellular vesicles as a potential biomarker for major depressive disorder. *Genes Dis* **2024**, *11*, 1009–1021.
5. Kennis, M.; Gerritsen, L.; van Dalen, M.; et al. Prospective biomarkers of major depressive disorder: A systematic review and meta-analysis. *Mol. Psychiatry* **2020**, *25*, 321–338.
6. Mayeux, R., Biomarkers: Potential uses and limitations. *Neurorx* **2004**, *1*, 182–188.
7. Sun, X.; Li, X.; Zong, P.; et al. f-p-d Orbital Hybridization Promotes Hydroxyl Intermediate Adsorption for Electrochemical Biomolecular Oxidation and Identification. *Anal. Chem.* **2025**, *97*, 880–885.
8. Tamilarasi, S.; Kumar, R.S.; Cho, K.-B.; Kim, C.-J.; et al. High-performance electrochemical detection of glucose in human blood serum using a hierarchical NiO_2 nanostructure supported on phosphorus doped graphene. *Mater. Today Chem.* **2023**, *34*, 101765.
9. Umapathi, S.; Masud, J.; Coleman, H.; et al. Electrochemical sensor based on CuSe for determination of dopamine. *Mikrochim. Acta* **2020**, *187*, 440.
10. Lei, Y.; Butler, D.; Lucking, M.C.; et al. Single-atom doping of MoS_2 with manganese enables ultrasensitive detection of dopamine: Experimental and computational approach. *Sci. Adv.* **2020**, 6, eabc4250.
11. Parker, J.G.; Marshall, J.D.; Ahanonu, B.; et al. Schnitzer, Diametric neural ensemble dynamics in parkinsonian and dyskinetic states. *Nature* **2018**, *557*, 177–182.
12. Chen, Y.; Gu, Y.; Wang, B.; et al. Synaptotagmin-11 deficiency mediates schizophrenia-like behaviors in mice via dopamine over-transmission. *Nat. Commun.* **2024**, *15*, 10571.
13. Hu, K.; Le Vo, K.L.; Wang, F.; et al. Single Exosome Amperometric Measurements Reveal Encapsulation of Chemical Messengers for Intercellular Communication. *J. Am. Chem. Soc.* **2023**, *145*, 11499–11503.
14. Cho, Y.W.; Park, J.H.; Lee, K.H.; et al. Recent advances in nanomaterial-modified electrical platforms for the detection of dopamine in living cells. *Nano Converg.* **2020**, *7*, 40.
15. Kimura, N.; Takayanagi, R.; Takizawa, N.; et al. Pathological grading for predicting metastasis in phaeochromocytoma and paraganglioma. *Endocr. Relat. Cancer* **2014**, *21*, 405–414.
16. Zhou, L.; Yang, R.; Li, X.; et al. COF-Coated Microelectrode for Space-Confined Electrochemical Sensing of Dopamine in Parkinson's Disease Model Mouse Brain. *J. Am. Chem. Soc.* **2023**, *145*, 23727–23738.
17. Monzani, E.; Nicolis, S.; Dell'Acqua, S.; et al. Oxidative Stress and Protein-Quinone Modifications in Parkinson's and Other Neurodegenerative Diseases. *Angew. Chem. Int. Ed. Engl.* **2019**, *58*, 6512–6527.
18. Huang, W.; Zhang, J.; Liu, D.; et al. Tuning the Electronic Structures of Multimetal Oxide Nanoplates to Realize Favorable Adsorption Energies of Oxygenated Intermediates. *ACS Nano* **2020**, *14*, 17640–17651.
19. Shi, J.; Guo, Y.H.; Xie, F.; et al. Redox-Active Ligand Assisted Catalytic Water Oxidation by a Ru(IV) =O Intermediate. *Angew. Chem. Int. Ed. Engl.* **2020**, *59*, 4000–4008.
20. Wang, Z.; Li, J.; Zhang, Q.; et al. Facilitating Formate Selectivity via Optimizing e(g)* Band Broadening in NiMn Hydroxides for Ethylene Glycol Electro-Oxidation. *Angew. Chem. Int. Ed. Engl.* **2024**, *63*, e202411517.
21. Ferreira, G.M.; Baptista, V.; Silva, V.; et al. CMOS Spectrophotometric Microsystem for Malaria Detection. *IEEE Trans. Biomed. Eng.* **2023**, *70*, 2318–2328.
22. Yamamoto, H.; Fujiwara, T.; Funatsu, T.; et al. Quantification of Intracellular Thiols by HPLC-Fluorescence Detection. *Molecules* **2021**, *26*, 2365.
23. Martinez, M.L.; Rodriguez, M.A.; Irazu, L.E.; et al. New enzyme-linked immunoassay for the detection of specific antibodies against multiple Leptospira serogroups in bovine sera. *Comp. Immunol. Microbiol. Infect. Dis.* **2021**, *75*, 101609.
24. Natarajan, B.; Kannan, P.; Maduraiveeran, G.; et al. Polymer nanocomposite-based biomolecular sensor for healthcare

monitoring. *Adv. Colloid Interface Sci.* **2025**, *343*, 103557.
25. Shafiq, F.; Rather, J.A.; Said, M.A.; et al. Fluorescent molecularly imprinted polymers: Design strategies and biomolecular sensing applications for healthcare monitoring. *Adv. Colloid Interface Sci.* **2026**, *348*, 103740.
26. Jan, A.; Batool, M.; Akram, S.; et al. Functionalized Graphene Quantum Dots (FGQDs): A review of their synthesis, properties, and emerging biomedical applications. *Carbon Trends* **2025**, *18*, 100442.
27. Yang, X.L.; Zhu, Q.H.; Zhang, G.H.; et al. On-site portable detection of gaseous methyl iodide using an electrochemical method. *Chem. Commun.* **2024**, *60*, 1168–1171.
28. Díaz-Fernández, A.; Ranallo, S.; Ricci, F., Enzyme-Linked DNA Displacement (ELIDIS) Assay for Ultrasensitive Electrochemical Detection of Antibodies. *Angew. Chem. Int. Ed. Engl.* **2024**, *63*, e202314818.
29. Wang, H.; Wang, Y.; Liu, S.; et al. Signal-on electrochemical detection of antibiotics at zeptomole level based on target-aptamer binding triggered multiple recycling amplification. *Biosens. Bioelectron.* **2016**, *80*, 471–476.
30. Li, R.; Guo, W.; Zhu, Z.; et al. Single-Site Sn-O-Cu Pairs with Interfacial Electron Transfer Effect for Enhanced Electrochemical Catalysis and Sensing. *Small* **2023**, *19*, e2300149.
31. Li, X.; Jiao, L.; Li, R.; et al. Biomimetic Electronic Communication of Iodine Doped Single-Atom Fe Site for Highly Active and Stable Dopamine Oxidation. *Small* **2024**, *20*, e2405532.
32. Huang, J.; Mensi, M.; Oveisi, E.; et al. Buonsanti, Structural Sensitivities in Bimetallic Catalysts for Electrochemical CO_2 Reduction Revealed by Ag-Cu Nanodimers. *J. Am. Chem. Soc.* **2019**, *141*, 2490–2499.
33. Peng, C.; Ma, J.; Luo, G.; et al. (111) Facet-oriented Cu_2Mg Intermetallic Compound with Cu_3-Mg Sites for CO_2 Electroreduction to Ethanol with Industrial Current Density. *Angew. Chem. Int. Ed. Engl.* **2024**, *63*, e202316907.
34. Feng, Y.; Li, Z.; Liu, H.; et al. Laser-Prepared CuZn Alloy Catalyst for Selective Electrochemical Reduction of CO_2 to Ethylene. *Langmuir* **2018**, *34*, 13544–13549.